J Geophys (1985) 58:82–91

Journal of Geophysics

# Notes on wave propagation in laterally varying structure

**D.V. Helmberger, G. Engen and S. Grand**
Seismological Laboratory, California Institute of Technology, Pasadena, California 91125, USA

**Abstract.** Recent models of earth structure suggest large horizontal gradients, especially in shear velocities. Some changes in existing methods are required to construct synthetics for broadband signals in many situations, especially when energy can reach the receiver by up-going as well as down-going paths. This can be accomplished by allowing locally dipping structure and making some modifications to generalized ray theory. Local ray parameters are expressed in terms of a global reference which allows a de Hoop contour to be constructed for each generalized ray with the usual application of the Cagniard-de Hoop technique. Several useful approximations of ray expansions and WKBJ theory are presented. Comparisons of the synthetics produced by these two basic techniques alone, or in combination with known solutions, demonstrates their reliability and limitations.

**Key words:** Synthetic seismograms – Generalized ray theory – WKBJ seismograms – Lateral heterogeneity

## Introduction

Considerable progress has been made recently in speeding-up the synthesizing of seismograms with the introduction of WKBJ and Gaussian beam methods, see Chapman (1978) and Červený et al. (1982). These methods have proven highly useful in generalizations to laterally varying structure, especially at high frequency, see for example Frazer and Phinney (1980). However, in the construction of longer periods (long-period WWSSN seismograms) we are often interested in more complete solutions, since the beginning portion of surface waves become important, see Grand and Helmberger (1984a). A complete set of ray parameter contributions is required to construct seismograms in this situation. In particular, one needs to consider ray paths leaving the source horizontally, a case where the WKBJ method breaks down. We can avoid this problem by applying a mixture of generalized ray theory, GRT, and WKBJ or Disk rays as defined by Wiggins (1976).

A simple example of this procedure is given in Fig. 1 where we show schematically how to construct the step response for a smooth velocity model approximated by a stack of homogeneous layers. We suppose that a velocity model can be chosen such that the step response remains a step at all receiver positions. The simulation of this step can be achieved by summing the response from three energy paths; namely, the direct, the reflected from just below the source or reference plane and the diving WKBJ contribution. All three paths contain a product of the transmission coefficients above the source. The WKBJ path includes the transmission coefficients across the reference plane, taken as the interface below the source. We have included a diagram of the $\theta(t)$ vs. $p$ curve in Fig. 1 for reference, as it clearly shows that the diving path contributes little except at the larger distances. At the nearest distance, position 1, the direct ray dominates. The reflected path contributes some as critical angle is approached. At still larger distances, position 3, a head wave along the bottom of the reference interface develops followed by the critically reflected pulse. The head wave contribution is included in the reflected response since it is associated with the reflected generalized ray. At large ranges, the WKBJ contribution becomes increasingly dominant. Note that the WKBJ response turns off at the same time as the head wave starts, because the transmission coefficient drops to zero. Essentially, combining the generalized rays and WKBJ response eliminates the truncation phase and avoids the turning point breakdown of the WKBJ theory.

In testing the accuracy of the above procedure, it is quite useful to generate the step response for models for which the answer is known. Thus, we begin with a homogeneous fluid whole space with a point source excitation yielding a step response at all positions with 1/(distance) decay. We next impose a spherical coordinate system with many thin shells of constant velocity. Applying the classical earth-flattening approximation, we obtain a model with a smooth velocity increase in depth, see Helmberger (1973). The synthetics generated in Fig. 2 are from such a model, with the exact step responses indicated by the dotted lines in the bottom panel. This panel also displays the response after summing the complete set of generalized rays; direct rays plus rays reflected upward from all the interfaces below the source. The GRT response at the largest distance shows the most roughness for times near the direct arrival when the interaction with the reflection from just below the source is the most severe. Similar complexity occurs with the hybrid method except that the diving energy is smoother with WKBJ. Short-period synthetics generated from these step responses become quite dirty and simple geometric ray theory yields cleaner results. However, for most studies the advantage of being able to include the radiation pattern

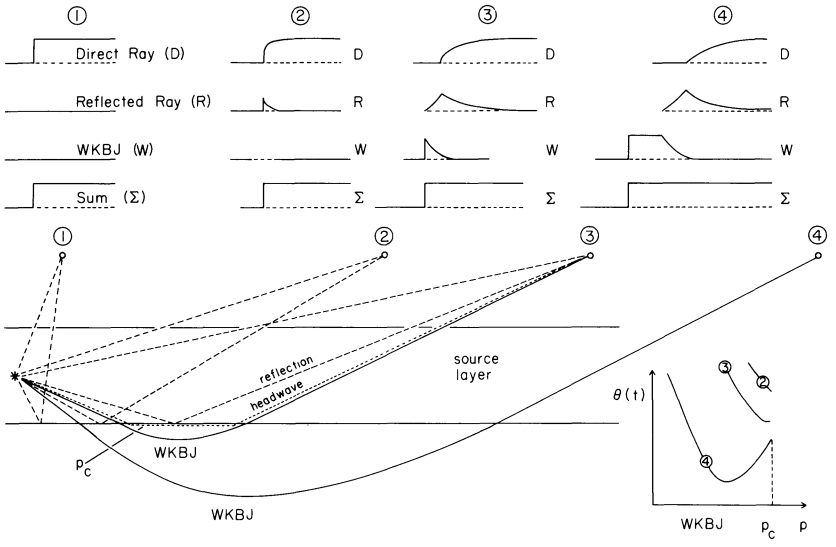


**Fig. 1.** Schematic picture of ray paths and summation response (also schematic) for a smooth velocity gradient specified by a layered stack. Reflected and head-wave paths for case 4 are omitted

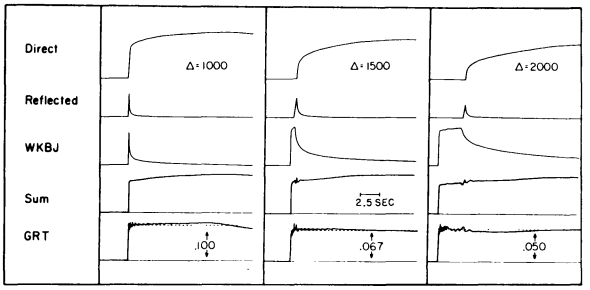


**Fig. 2.** Synthetic step responses computed at three interesting distances and constructed by summing the three energy paths displayed in Fig. 1. The exact answer is indicated by the *dotted response in the lower panel*

appropriate for earthquake sources, or shear dislocations, far outweighs the disadvantage of the noise generated by the hybrid method. For example, consider the $SH$ radiation from a dip-slip event where the up-going radiation has opposite polarity from the down-going energy, see Helmberger (1973). In short, the sum as displayed in Fig. 2 becomes more interesting when the direct ray trace has opposite sign from the other two.

We could probably improve the response at the time the three energy paths interfere most vigorously by including a few more GRs and/or by lowering the reference boundary for the WKBJ contribution. However, we are particularly interested in more realistic earth models with a sedimentary cover over bedrock or a crust-over-mantle structure providing natural reference boundaries. Thus, we propose using GRs to compute the start of the Love waves, and WKBJ to generate the responses returning from deeper structure. This approach proved effective in studying the structure and evolution of the lithosphere for an old oceanic plate, Grand and Helmberger (1984b). It would be advantageous to treat the obvious lateral variation encountered in such studies. Although the real world is truly three-dimensional, some useful progress can be made by examining profiles of data along paths of symmetry where two-dimensional idealizations are appropriate. We will address such models in this paper.

Our strategy is similar to Wiggins (1976) and Given (1984) in that we will use a combination of GRT and WKBJ to generate synthetics and justify the latter by demonstrated accuracy.

## Review of ray interactions with nonplanar structure

Boundary-value problems involving complicated geometry have a long, rather unrewarding history; thus, we will jump directly to approximate solutions and test their validity against finite-difference calculations and other more well-known results. Before addressing the dipping layer problem, it is instructive to examine the flat-layered case and emphasize the geometric interpretation of generalized ray theory. This proves particularly useful for constructing generalizations to more complicated situations since the most progress in understanding these problems is at high frequency. Both line and point sources will be discussed since the former is easier to understand theoretically and for testing against numerical results, while the latter is necessary for studying the Earth.

### *Line source and planar model*

The solution of the scalar wave equation, assuming line source excitation for generalized rays, as given by Gilbert and Knopoff (1961), is

$$\Phi_L(r, z, t) = H(t-t_0)/(t^2-t_0^2)^{1/2} \tag{1}$$

where $t_0 = R/\alpha$, $R^2 = z^2 + r^2$, and $\alpha$ = velocity.

$\Phi_L$ is defined as the displacement potential with the index $L$ used to remind ourselves of the line excitation. A high-frequency approximation of Eq. (1) is

$$\Phi_L \propto H(t-t_0)/(t-t_0)^{1/2}\sqrt{R} \tag{2}$$

and the motion decays with distance as $\sqrt{R}$. The solution to the interface problem setup displayed in Fig. 3a is

$$\Phi_L(r, z, t) = \mathrm{Im}\left[\frac{1}{\eta_1}\frac{dp}{dt}T(p)\right] \tag{3}$$

where

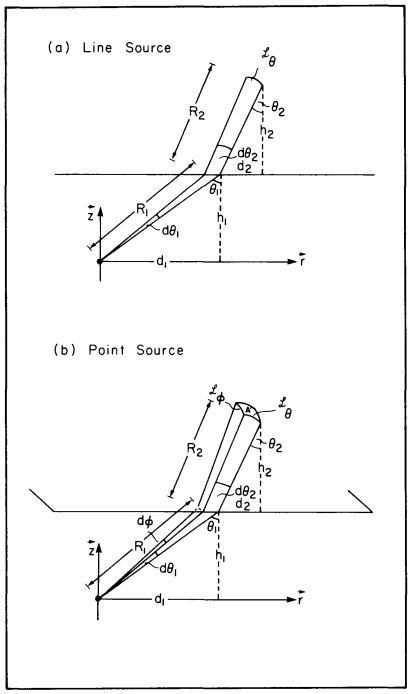


**Fig. 3.** Diagram displaying the geometric spreading of ray tubes in two and three dimensions as they encounter a boundary

$$t = p(d_1 + d_2) + h_1\,\eta_1 + h_2\,\eta_2 \tag{4}$$

$$\eta_i = \left(\frac{1}{\alpha_i^2} - p^2\right)^{1/2}.$$

$T(p)$ = transmission coefficient.

The symbol Im indicates the imaginary part of the complex product of the functions of ray parameter, see Helmberger (1983) for example. The ray parameter appropriate for the direct arrival path, $p_0$, can be obtained by

$$\frac{dt}{dp}(p_0) = 0, \quad \text{and} \quad d_1 - \frac{h_1 p_0}{\eta_1} = d_2 - \frac{h_2 p_0}{\eta_2}. \tag{5}$$

But with

$$p_0 = \frac{\sin\theta_1}{\alpha_1} = \frac{\sin\theta_2}{\alpha_2} \tag{6}$$

and, therefore,

$$\eta_1 = \frac{\cos\theta_1}{\alpha_1}, \qquad \eta_2 = \frac{\cos\theta_2}{\alpha_2},$$

we see that the ray goes from the source to the receiver. And

$$t_0 = \left\{\frac{\sin\theta_1}{\alpha_1} r_1 + \frac{\cos\theta_1}{\alpha_1} h_1\right\} + \left\{\frac{\sin\theta_2}{\alpha_2} d_2 + \frac{\cos\theta_2}{\alpha_2} h_2\right\}, \tag{7}$$

$$t_0 = R_1/\alpha_1 + R_2/\alpha_2.$$

For times greater than $t_0$, we must solve $t$ for complex $p$ such that the imaginary parts of $p d_1$ and $\eta_1 h_1$ etc. cancel.

The behavior near $p$, can be approximated by noting that

$$t = r_0 + \frac{dt}{dp}(p - p_0) + \frac{d^2t}{dp^2}(p - p_0)^2/2$$

and solving for

$$(p - p_0)^2 = 2(t - t_0) \left(\frac{d^2t}{dp^2}\right).$$

Thus,

$$\frac{dp}{dt} = (t - t_0)^{-1/2} \left(2\frac{d^2t}{dp^2}\right)^{1/2}. \tag{8}$$

Note that from Eq. (4)

$$\frac{d^2t}{dp^2} = \frac{-h_1}{\eta_1^3 \alpha_1^2} - \frac{h_2}{\eta_2^3 \alpha_2^2} \tag{9}$$

It is convenient to condense the various factors containing $p_0$, into

$$S_L(p_0) \equiv \frac{1}{\left|\frac{d^2t}{dp^2}\right|^{1/2} \sqrt{\alpha_1}\,\eta_1}, \tag{10}$$

which we call the spreading factor. Thus,

$$S_L = \left[\frac{h_1}{\eta_1 \alpha_1} + \frac{h_2}{\eta_2 \alpha_2}\left(\frac{\eta_1^2 \alpha_1}{\eta_2^2 \alpha_2}\right)\right]^{-1/2}. \tag{11}$$

We note that by differentiating Snell's law we obtain

$$\frac{\cos\theta_1}{\alpha_1} d\theta_1 = \frac{\cos\theta_2}{\alpha_2} d\theta_2.$$

Substituting this expression into $S_L$ we obtain

$$S_L = \frac{\sqrt{d\theta_1}}{\left[R_1\, d\theta_1 + R_2\, d\theta_2 \frac{\cos\theta_1}{\cos\theta_2}\right]^{1/2}}. \tag{12}$$

If $R_2 = 0$, we obtain the whole-space spreading again where $(R_1\, d\theta_1)$ is just the width of the ray tube described in Fig. 3a. A correction for the change in direction is required as the tube crosses the interface, namely

$(\cos\theta_1/\cos\theta_2)$.

Thus, the denominator of Eq. (12) is again the width of the ray tube at the receiver, $L_\theta$ in Fig. 3a. Substituting into Eq. (3) we obtain

$$\Phi_L \propto S_L\, H(t - t_0)\, \mathrm{Re}[T(p_0)]/(t - t_0)^{1/2} \tag{13}$$

where Re indicates the real part operator.

*Point source and planar model*

The point-source solution for the same problem setup, Fig. 3b, is

$$\Phi_p(r,z,t)=\sqrt{\frac{2}{r}}\frac{1}{\pi}\left[\frac{1}{\sqrt{t}} * \mathrm{Im}\left(T(p)\frac{\sqrt{p}}{\eta_1}\frac{dp}{dt}\right)\right] \tag{14}$$

and applying the same first-motion approximation, we obtain a slightly more complicated spreading factor; namely

$$Sp\equiv\sqrt{\frac{p}{r}}\frac{1}{\eta_1}\left|\frac{d^2t}{dp^2}\right|^{-1/2} \tag{15}$$

$$=\left[\frac{R_1\sin\theta_1+R_2\sin\theta_2}{\sin\theta_1}\right]^{-1/2}S_L \tag{16}$$

and note that by letting $R_2=0$ we obtain

$$S_P=1/R. \tag{17}$$

In terms of area, we note that

$$S_P=\left[\frac{\sin\theta_1\,d\theta_1\,d\Phi}{(R_1\sin\theta_1\,d\Phi+R_2\sin\theta_2\,d\Phi)\left(R_1\,d\theta_1+R_2\,d\theta_2\frac{\cos\theta_1}{\cos\theta_2}\right)}\right]^{1/2} \tag{18}$$

which can be interpreted as the incremental element of area at the source divided by the projected area at the receiver, or simply

$$S_P=\left(\frac{A_0}{A}\right)^{1/2}. \tag{19}$$

Thus, the first-motion behavior becomes

$$\Phi_1(r_1\,t_1\,t)=\frac{1}{\pi}\left[\frac{1}{\sqrt{t}} * \frac{1}{\sqrt{t-t_0}}\right]S_P\,\mathrm{Re}[T(p_0)]$$
$$=S_p\,H(t-t_0)\,\mathrm{Re}[T(p_0)]. \tag{20}$$

More complicated solutions to multi-layered models in terms of ray summations will be discussed later.

*Locally dipping structure*

Although GRT for parallel interfaces has been well developed, the modifications for nonplanar structure or smoothly varying interfaces has not. Some of the difficulties encountered for the simple wedge problem have been discussed by Hudson (1963). Hong and Helmberger (1977) constructed a solution in terms of generalized rays for this problem and defined a method of ray-path construction compatible with the usual Cagniard-de Hoop formalism. We will consider the direct arrival interacting with two dipping interfaces as an example application. The problem setup is displayed in Fig. 4a with the response given by

$$\Phi_L=\mathrm{Im}\left[T_{12}(p_1)\,T_{23}(p_2)\frac{1}{\eta_1}\frac{dp}{dt}\right] \tag{21}$$

where $p_1$ and $p_2$ are defined by the local ray parameter, namely

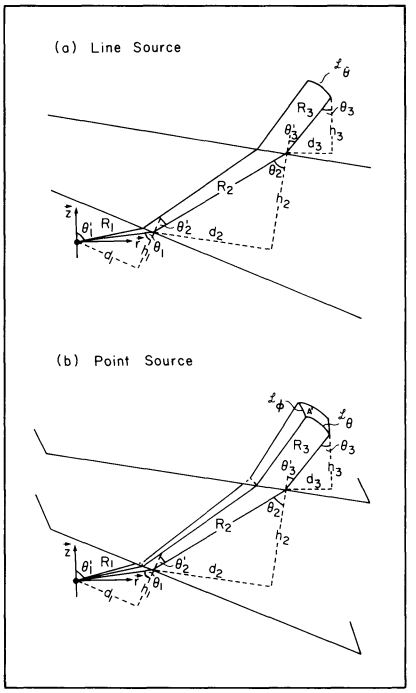


**Fig. 4.** Diagram displaying the geometric spreading of rays encountering nonhorizontal interfaces

$$p_1=\frac{\sin\theta_1}{\alpha_1},\qquad p_2=\frac{\sin\theta_2}{\alpha_2}$$

and are no longer equal. However,

$$\frac{\sin\theta_1}{\alpha_1}=\frac{\sin\theta_2'}{\alpha_2}$$

where

$$\theta_2'=\theta_2+\theta_s$$

with $\theta_s$ defining the change of the slope of interface (1) relative to the previous reference at $\theta_1$. Performing the derivatives discussed in the previous section, we obtain

$$S_L(p_0)=\frac{\sqrt{d\theta_1}}{\left[R_1\,d\theta_1+R_2\,d\theta_2\frac{\cos\theta_1}{\cos\theta_2'}+R_3\,d\theta_3\frac{\cos\theta_2}{\cos\theta_2'}\frac{\cos\theta_1}{\cos\theta_2'}\right]^{1/2}}$$

which is similar to Eq. (12) and has the same interpretation. The travel time is defined by

$$t=\sum_{i=1}^{3}(p_i\,d_i+\eta_i\,h_i) \tag{22}$$

with the definitions of $d_i$ and $h_i$ given in Fig. 4a as the projection of the geometric path onto the local Cartesian coordinates. The arrival time can be determined as before, with

$$\frac{dt}{dp_m}=0$$

defining

$p_1 = p_{0_1}$, $p_2 = p_{0_2}$,

etc.. Thus,

$$d_m - h_m \frac{p_m}{\eta_m} = 0 \tag{23}$$

with

$$p_m = \frac{\sin\theta_m}{\alpha_m} \quad \text{and} \quad \eta_m = \frac{\cos\theta_m}{\alpha_m}$$

and the $\frac{dt}{dp_m} = 0$ condition leads to a ray going from the source to the receiver. The first-motion approximation becomes

$$\Phi_L \propto \mathrm{Re}[T_{12}(p_{0_1}) T_{23}(p_{0_2})] \frac{H(t-t_0)}{(t-t_0)^{1/2}} S_L. \tag{24}$$

Spreading for the point-source solution becomes slightly more complicated than in the flat case, but allowing

$$\sqrt{\frac{r}{p}} = \left(\sum_{i=1}^{3} \frac{d_i}{p_i}\right)^{1/2} \tag{25}$$

results in $S_p$, defined by

$$S_p = \sqrt{\frac{p}{r}} \frac{1}{\eta_1} \left|\frac{d^2 t}{dp^2}\right|^{-1/2}, \tag{26}$$

reducing to

$$= (A_0/A)^{1/2},$$

at the direct arrival time. The details of this result have been given previously by Hong and Helmberger (1978). Thus, the point-source solution for the geometry given in Fig. 4b becomes

$$\Phi_p = \frac{1}{\pi} \left\{ \frac{1}{\sqrt{t}} * \mathrm{Im}\left[ \Pi(p) \frac{1}{\eta_1} \frac{dp}{dt} \left[ \sum \left(\frac{d_i}{p_i}\right) \right]^{-1/2} \right] \right\}, \tag{27}$$

where

$$\Pi(p) = T_{12}(p_1)\, T_{23}(p_2).$$

Numerical evaluation of Eq. (27) yields the geometric result but, also, retains longer-period information since $(dp/dt)$ can be evaluated along the de Hoop contour in the usual manner. The accuracy of constructing broadband synthetics applying this procedure is well known: for example see Apsel and Luco (1983) or Burdick and Orcutt (1978).

*Many layers, WKBJ and radiation patterns*

Following the results of the previous section, and inserting the radiation pattern for the simple $SH$ motions from a dislocation source (see Helmberger and Malone, 1975, the displacements can be written

$$v(r, z, \theta, t) = \frac{M_0}{4\pi\rho_0} \left(\frac{\Delta}{\sin\Delta}\right)^{1/2} \frac{d}{dt} \left[ \dot{D}(t) * \sum_{j=1}^{2} A_j(\theta, \lambda, \delta)\, V_j(t) \right], \tag{28}$$

where

$$V_j(t) = \sqrt{\frac{2}{r}} \frac{1}{\pi} \left[ \frac{1}{\sqrt{t}} * \Psi_j(t) \right] \tag{29}$$

and

$$\Psi_j(t) = \sum_{i=1}^{n} SH_j(p) \frac{\sqrt{p}}{\eta_\beta} (2p)\, C_s \frac{dp}{dt}\, \Pi_i(p) \tag{30}$$

and the summation of $n$ rays is required. The various symbols are defined below:

$v(r, z, \theta, t)$ = displacement on free surface
$M_0$ = moment
$p_0$ = density
$D(t)$ = dislocation history
$\dot{D}(t)$ = far-field time function
$A_1(\theta, \lambda, \delta) = \cos 2\theta \cos\lambda \sin\delta - 1/2 \sin 2\theta \sin\lambda \sin 2\delta$,
$A_2(\theta, \lambda, \delta) = -\sin\theta \cos\lambda \cos\delta - \cos\theta \sin\lambda \cos 2\delta$,
$\theta$ = strike from the end of the fault plane
$\lambda$ = rake angle
$\delta$ = dip angle
$r$ = distance between source and receiver
$p$ = ray parameter
$\eta = \left(\frac{1}{\beta^2} - p^2\right)^{1/2}$
$\Delta$ = epicentral distance in radians
$\left(\frac{\Delta}{\sin\Delta}\right)^{1/2}$ = correction for earth flattening
$\beta$ = shear velocity

and where the vertical radiation patterns are given by

$$SH_1 = \frac{1}{\beta^2},$$

$$SH_2 = \frac{\varepsilon}{\beta^2} \frac{\eta}{p}, \qquad \varepsilon = \begin{matrix} +1 & z > h \\ -1 & z < h \end{matrix}$$

$$\eta = \left(\frac{1}{\beta^2} - p^2\right)^{1/2}.$$

The correction for point-source spreading is defined by

$$C_s = \sqrt{\frac{r}{p}} \left(\sum \frac{d_i}{p_i}\right)^{-1/2}. \tag{31}$$

This solution is similar to the flat case and we can, obviously, construct the diving ray response for a smoothly varying structure by summing the primary rays as discussed in Fig. 2. We can then use this result to check the disk ray solution which can be obtained by replacing Eq. (30) by

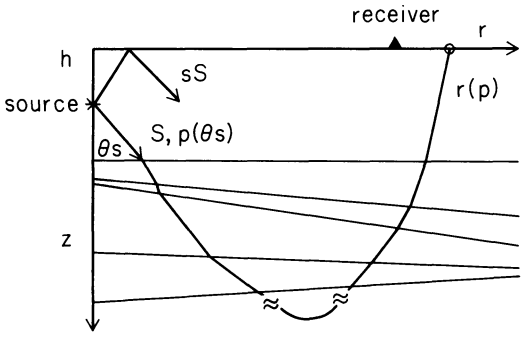


**Fig. 5.** Ray geometry where the source and receiver are separated by $r$ and the source depth is $h$. The ray starts with the $p=\sin\theta_s/\beta$ and reaches the surface at $r(p')$ where the ray parameter along the path has been adjusted according to the local dipping structure

$$\psi_j = SH_j(p)\frac{\sqrt{p}}{\eta_\beta}(p)\sum(\delta p/\delta t) \tag{32}$$

where the sum is taken over the $p(t)$ curve as described by Wiggins (1976).

For a simple turning ray problem,

$$\left|\frac{\delta p}{\delta t}\right| = \frac{1}{|r-r(p)|} \tag{33}$$

where $r(p)$ is distance reached by a ray defined by $p$, see Fig. 5. Substituting Eq. (33) into Eq. (32) and evaluating Eq. (29) yields a simple step response, as discussed by Chapman (1976). Essentially, Eq. (33) has a simple square-root singularity at $r=r(p)$, and rays that hit the surface near the receiver dominate the behavior. Since $p$ varies along the path, we must define which $p$ to use in the evaluation of Eq. (32). The proper choice is the starting $p$ at the source as outlined in the previous section. Note that for the case of an up-going direct ray the two methods can be interpreted in a similar manner. Only one ray is involved in both, and applying the first-motion approximation of Eq. (30) yields Eq. (32) where the extra factor 2 is produced by the double-valued nature of expression (33). Thus, the application of WKBJ theory to the locally dipping problem appears to be essentially the same as for the uniform-layered problem. We trace the ray through a stack of layers down to the turning region, turn it around analytically, and follow it to the surface obeying Snell's law. The special treatment at the turning point removes the nonlinear ray parameter effects of the homogeneous-layered parameterization as is well known. Essentially, when the ray reaches critical angle at a given interface, we back up to the previous reference interface and compute the local linear velocity gradient. The travel time and location at which the ray recrosses the reference interface is easily calculated by analytical means. Such a procedure is compatible with the Langer approximation which is the basis for the WKBJ method, see Aki and Richards (1980). Earth stretching becomes slightly more complicated than in the uniform-layered case. In this situation we let

$$ra_j = (r_j + r_{j+1})/2$$

where $r_j$ is the radius of the Earth at the $j$-th layer, etc., and $ra_j$ becomes the radius at the midpoint of the layer. The cross-section is then constructed in terms of vertical profiles of velocity and thickness vs. $ra_j$ and the points connected by linear lines as displayed in Fig. 5. Next, the layer thicknesses, $Th_j$, are increased by

$$r_j = Th_j(r_0/ra_j)$$

where $r_0$ is the radius of the Earth. This approximation is adequate for shallow depths. A better transformation for deeper depths is given by Müller (1971). Note that at this stage the horizontal velocity in each layer remains constant. The velocity-depth cross-sections will be presented in this format. The velocity and density approximations are determined as the ray encounters the various interfaces with

$$\beta = V_j(r_0/ra_j)$$

$$\rho_j = d_j(r_0/ra_j)$$

and $ra_j$ is determined by the local layer thickness and position. Thus, the velocity is no longer constant in any given layer but depends on local depth correction. The $C_s$ factor can be assumed to be one for most applications of gentle dipping structure, as discussed in the next section and was omitted from Eq. (32).

The approach followed here is similar to that followed by Wiggins (1976) in that the main justification for expression Eq. (33) is that it yields results comparable to GRT. A theoretical justification of applying WKBJ to laterally varying structure is given by Chapman and Drummond (1982). See Wesson (1970).

## Applications

In this section we will briefly outline possible applications of these approximate solutions to seismological problems. First, the direct or up-going energy problem is discussed when motions in the sloping layers of a sedimentary basin are excited by a line source. In this form, finite-difference calculations can be used to check the accuracy of the GRT results. Next, the point-source excitation of Love waves is considered in the presence of sloping structure followed by models of growing lithosphere. Finally, we construct synthetics for laterally varying upper-mantle models and confirm the usefulness of WKBJ at long periods.

### *Local seismograms*

One of many complexities associated with strong-motion seismology is the noticeably long duration of high-frequency $P$ waves observed in sedimentary basins. These waves are generally polarized onto the vertical component due to the strong velocity gradients near the surface. The latter portion of these observed motions are generally depleted at lower frequency. Thus, one might conclude that there are propagational waveguides that preferentially prolong high-frequency motions. Non-planar surface layering appears to have this property. This calculation will be done with $SH$ waves since this type of motion is studied throughout the remainder of this paper, but we would expect that $P$ waves would behave in a similar manner.

A single low-velocity layer which grows with distance between the source and receiver is assumed with a line source of $SH$ motion situated at a depth of 5.5 km. The

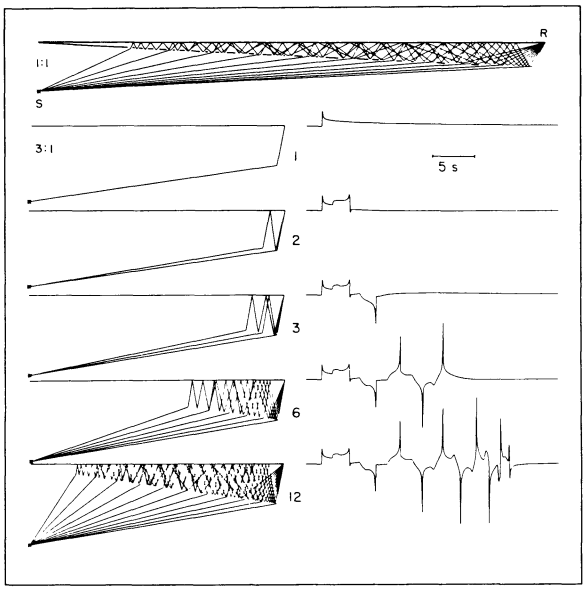


**Fig. 6.** Line-source response as a function of generalized ray summation. The seismic parameters are $\beta_1 = 1.5$ km/s, $\rho_1 = 1.5$ gm/c$^3$, and $\beta_2 = 3.3$, $\rho_2 = 2.5$ for the upper and lower layer, respectively. The *top plot* displays the ray paths at ray parameters appropriate for Snell's law at true scale. Ray plots *on the left* have a vertical exaggeration of 3 to 1

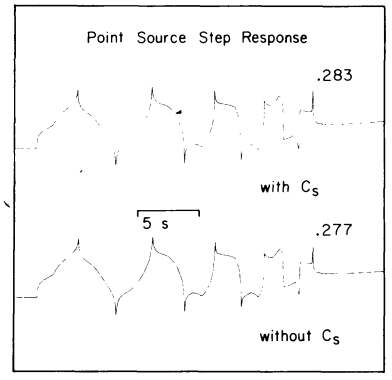


**Fig. 7.** Step responses appropriate for a strike-slip double couple source and the model discussed in Fig. 6 with and without the $C_s$ correction. The numbers above each trace indicate the peak amplitude

response build-up as a function of the number of multiples is displayed in Fig. 6. The square-root singularity indicated in expression (13) is apparent for the direct arrival. Note that after one bounce the reflection from the lower interface becomes complex because of the local ray parameter effect and a head wave and post-critical angle reflection develops. After two bounces, the time separation between the head-wave onset and reflection times becomes less and the reflected spike increases in strength. After many bounces the ray can no longer reach critical angle and still fit into the waveguide. Thus, $(R)^n$ becomes small since the reflection coefficient $(R)$ becomes less than one. The drop-off in amplitude of the multiples occurs abruptly at this time on the record.

The corresponding point-source response displayed in Fig. 7 can be obtained from expression (29). Neglecting the $C_s$ factor produces a similar response with a slight reduction

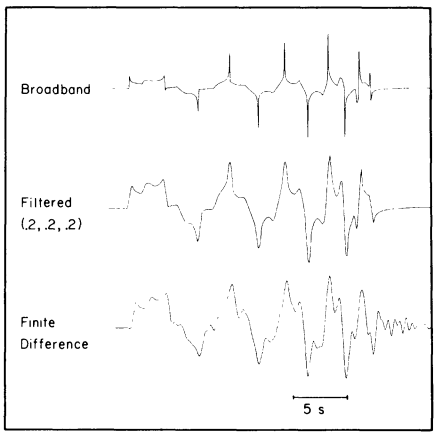


**Fig. 8.** Comparison of GRT results with a finite-difference calculation. The broadband trace has been filtered to remove the high-frequency spikes

in later arrivals, roughly 13% for the last arrival. Thus, point-source amplitudes can be approximated quite well by scaling line-source results by the square-root of the distance factor similar to the flat case. Note that the Cagniard-de Hoop technique proves particularly useful in tracing these rays and evaluating their individual contributions. However, as mentioned earlier, this series of rays does not necessarily converge to the exact solution and some demonstration of accuracy is required. This was attempted earlier by Hong and Helmberger (1977), but not very convincingly. A much more rigorous comparison with a numerical code is presently being conducted by Vidale et al. (1984) with preliminary results of the comparison of the two techniques for this simple model displayed in Fig. 8. The top trace is the broadband result displayed in Fig. 6, with a filtered response in the middle for comparison with finite-difference results on the bottom. The highest frequencies have been removed in this comparison due to computational expense but the existence of strong high-frequency multiples is striking. Since the finite-difference calculation can be performed on any arbitrary two-dimensional structure, we have extended the thin layer directly above the source to the left as a flat thin layer avoiding the wedge effect which is obviously omitted in the ray solution. Comparison with and without the wedge and many other complexities involving double-couple solutions constructed by line-to-point source operators are discussed in Vidale et al. (1984). We will suppose throughout the remainder of this paper that the generalized ray modifications discussed in the previous section are sufficiently accurate to test the WKBJ synthetics.

### *Love waves at regional distances*

Another interesting application of the above technique is in the development of Love waves and the effects of traveling across oceanic-to-continental transitions. This problem was encountered in a recent paper by Grand and Helmberger (1984b) when the so-called *G* phase, the name applied to the impulsive Love waves associated with oceanic paths, interferes with mantle arrivals. Apparently, this situation occurs for well-developed lithosphere associated with older plates over-lying slower upper-mantle velocity models. The beginning portions of the *G* phase, as recorded slightly inland, develop longer periods than observed at

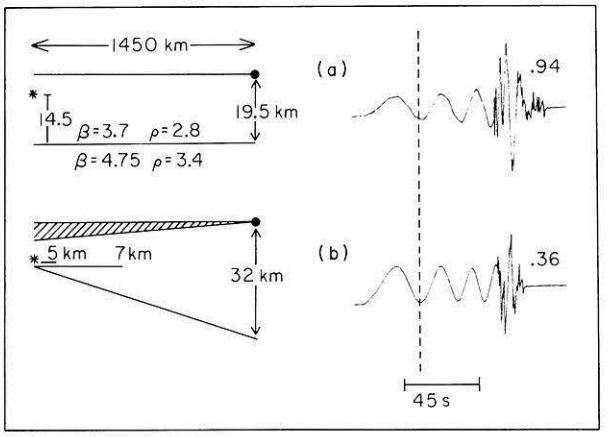


**Fig. 9.** Flat and dipping models and corresponding step responses with peak amplitudes indicated on each trace. Note that the first 45 s of each record are nearly identical in amplitude and shape when corrected by the scaling factors. The *shaded area* indicates the water layer

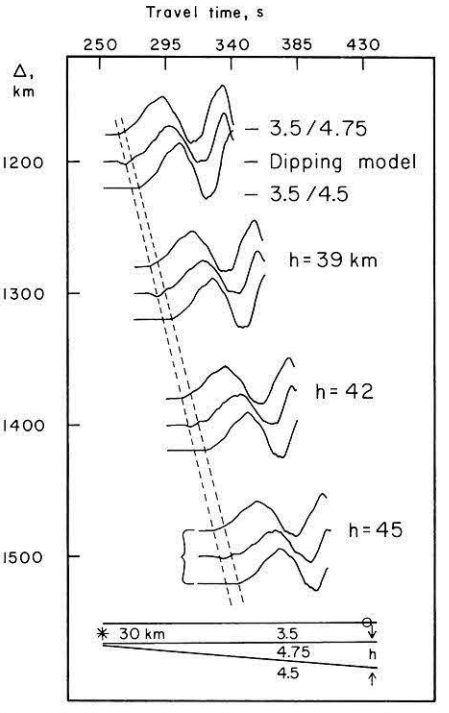


**Fig. 10.** Comparison of step responses for two simple models with a model containing a growing high-velocity lid. The *dotted lines* indicate the first arrival times of the two simple models

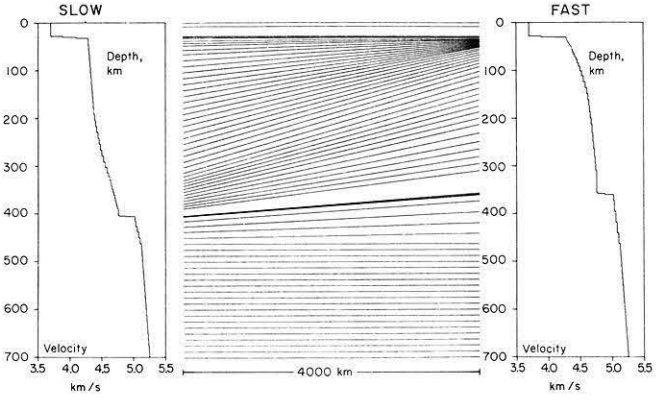


**Fig. 11.** Cross-section displaying isovelocity lines and accompanying starting and ending model

island stations. Their period and arrival times are compatible with the model presented in Fig. 9a. A dipping model with arrival times compatible with the flat model is presented in Fig. 9b along with the comparison of step responses given on the right. Note that the first 45 s of motion are nearly identical. The higher-frequency portions of the Love wave become less pronounced in the dipping case but the general appearance is similar to the pure-oceanic case, see Grand and Helmberger (1984b).

It appears that as the lithosphere ages it gets thicker; for example, see Forsyth (1975). A preliminary model of predicted Love waves for this situation is given in Fig. 10; also included are synthetics for a fast and slow mantle. The long-period nature of the synthetics from the dipping model is similar to the slow model as we might expect. However, there is considerable roughness at the start of the Love waves caused by the mixed paths involving both the crust and lid.

Observationally, we see upper-mantle arrivals starting near these ranges. Thus, the diving energy must be added to these synthetics following the strategy discussed earlier. This can be accomplished by summing GRs or by applying WKBJ.

*Upper-mantle models*

In this section we investigate effects of lateral variation in upper-mantle models, as displayed in Fig. 11. We have chosen a particularly simple case with no low-velocity zone to simplify the comparison of GRT with WKBJ synthetics. A further simplification is made by allowing the two models to be connected in a linear fashion as displayed in the middle column.

Following the WKBJ approach, we first illuminate the model by tracking a set of rays from the source towards prospective receivers. These rays reach the surface at $r(p)$ in time $T(p)$. The travel time at a particular receiver, $r$, can be written $t(p)=pr+T(p)-pr(p)$. Note that $p$ changes in each layer but they are all functions of the beginning $p$. Thus, we can construct the $t$ vs. $p$ curves as displayed in Fig. 12 for reversed profiles. The largest ray parameter, $p_{max}$, is 0.26 which corresponds to the crustal velocity of 3.9. Next, we perform the numerical derivative $(\delta p/\delta t)$ of these curves. Note that there will be a large truncation phase at the near stations at $p_{max}$. This can be avoided by including the product of the transmission coefficients, TCs, across the Moho, the reference interface discussed earlier, since $TC(p_{max})$ is small. Thus, the product of the TCs with $(\delta p/\delta t)$ has a relatively smooth behavior. The head wave along the Moho is added in by including the reflected generalized ray. By performing the convolution indicated in expression Eq. (29), we derive step responses from $t$ vs. $p$ curves displayed in Fig. 12. These results are shown in Fig. 13. Short-period synthetics are included to emphasize the rapid decay of amplitude at the triplication tips. Eliminating the truncation phase discussed here can also be achieved by a modification of the Gaussian beam technique as developed by Madariaga and Papadimitriou (1985).

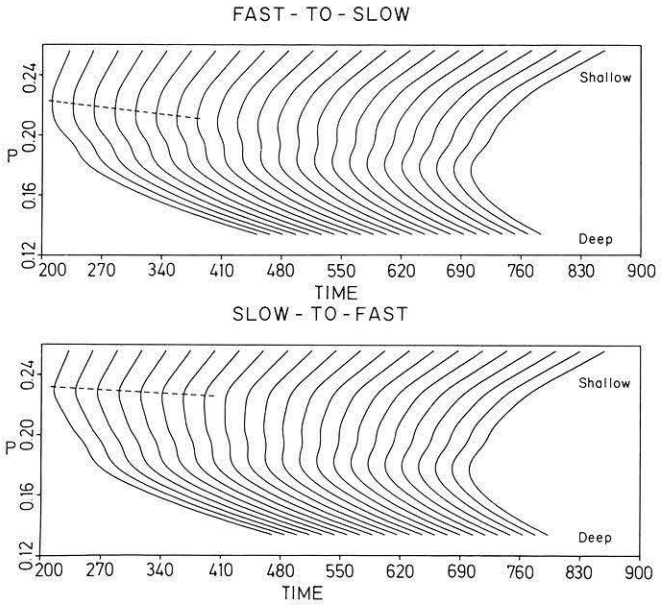


**Fig. 12.** Sets of $p$ vs. $t$ curves for possible receivers along a profile from 8° to 30°

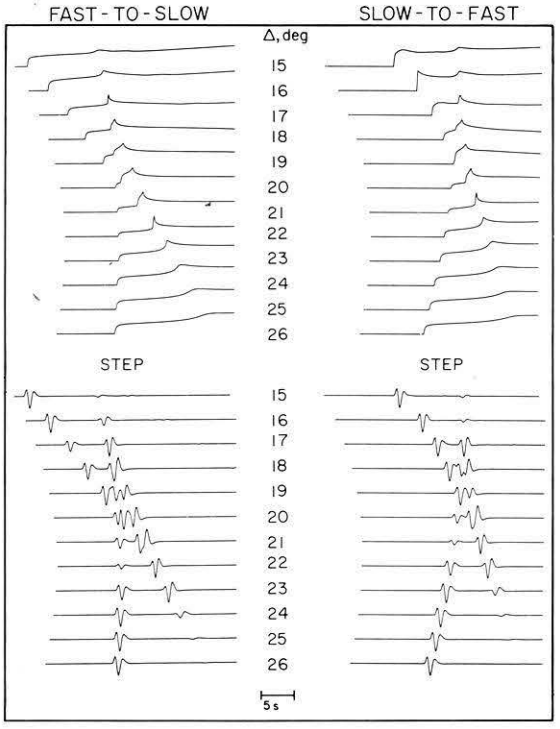


**Fig. 13.** Seismic sections plotted on the same reduced time scale. $r-\Delta/(5.4$ km/s). The synthetics are appropriate for a short-period WWSSN instrument response

The synthetics at the smallest ranges are completely controlled by the shallow structure and the local model. Thus, the first arrival from the fast-to-slow synthetics has a shorter travel time which causes the triplication from the 400-km discontinuity to arrive later than in the reverse profile.

A more detailed plot of the slow-to-fast profile is displayed in Fig. 14 along with the GRT responses for comparison. The synthetics are appropriate for the WWSSN

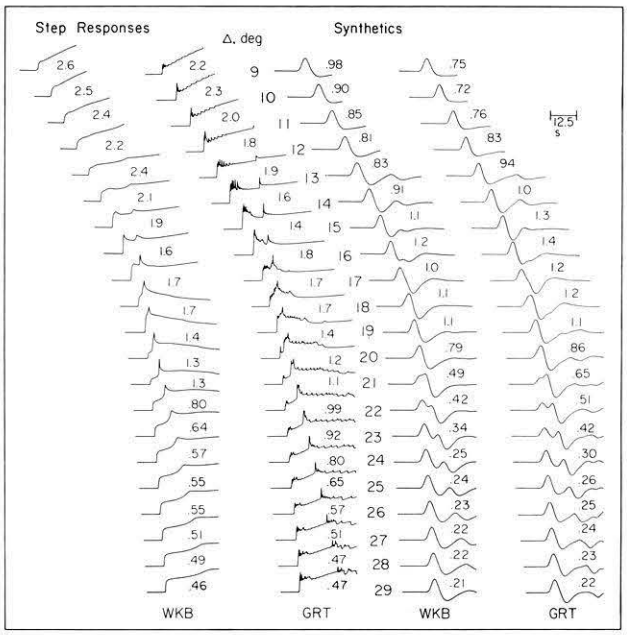


**Fig. 14.** Step responses and synthetics generated by the WKBJ and GRT methods for the slow-to-fast model displayed in Fig. 11. The numbers associated with each trace indicate the maximum amplitude

long-period system. A typical strike-slip source was assumed with a triangular time history of (1, 1, 1 s) and a $t^*=3$ s, see Grand and Helmberger (1984a).

Note that there is a distinct change in the latter portion of the WKBJ step responses between 17° and 18°. This is caused by omitting the head waves from along the top of the model for distances beyond 17°. However, no apparent change in the synthetics occurs at this range, suggesting that the long-period drift is outside the pass-band of the operators used in generating these synthetics. The high-frequency spikes so apparent in the GRT step responses are likewise removed by the convolution operators.

The 400-km discontinuity is treated slightly differently in the two methods, which leads to some shifts in the triplication position. In GRT, the 400-km discontinuity is generally treated as a sharp jump in velocity since this leads to the best results when compared against reflectivity, see Burdick and Orcutt (1978). On the other hand, WKBJ requires a smooth transition, 3-km transition in this particular case, such that the $p$ vs. $t$ curve is smooth. Thus, the sharp spikes occurring in the GRT step responses near 14° are precritical-angle reflections from the 400-km discontinuity. Similarly, the triplication seems to extend to greater distances in the GRT results. Note that the most severe mismatch occurs near this range. At larger ranges the two methods agree quite well, especially the synthetic waveforms. In fact, the synthetic waveforms agree at all distances with the maximum deviation in amplitude of about 25%. Since these synthetic waveforms are used to interpret observations which can seldom be modeled as well as the agreement between these two methods, we can consider the WKBJ modifications successful. For more precision involving sharp boundaries, we suggest breaking the $p$ integration into a combination of WKBJ for the smooth portion of the model and a generalized ray for the reflecting interface, for example see Given (1984).

## Conclusions

In this paper we presented a hybrid procedure of generating complete seismograms in laterally varying structure by applying a mixture of GRT and WKBJ methods. First, we reviewed the modifications of GRT required for dipping structure in terms of local coordinates and ray parameter concepts for line- and point-source theory. Solutions calculated by this approach not only agree with geometric results, but also agree with longer-period motions such as computed with finite-difference methods. Using the correspondence between GRT and WKBJ theory, we can express the latter in relatively simple form, essentially applying a square-root of distance correction to line-source spreading. Comparisons between GRT and WKBJ synthetics of diving energy paths agree reasonably well. Thus, we can construct nearly complete seismograms with a combination of GRT and WKBJ , with the former used to handle the shallow structure. Some useful demonstrations of the methods are given for crustal and upper-mantle models

*Acknowledgements.* We would like to thank Cindy Arvesen for helping with the drafting. This work was supported by ONR No. N00014-76-C-1070 and by the Air Force Geophysics Laboratory, Hanscom, Massachusetts, No. F19628-83-K-0010. Contribution 4155, Division of Geological and Planetary Sciences, California Institute of Technology, Pasadena, California 91125.

## References

Aki, K, Richards, P.G.: Quantitative seismology, theory and methods. W.H. Freeman and Company 1980

Apsel, R.J., Luco, J.E.: On the Green's functions for a layered halfspace, Part II. Bull. Seismol. Soc. Am. **73**, 931–952, 1983

Burdick, L.J., Orcutt, J.A.: A comparison of the generalized ray and reflectivity methods of waveform synthesis. Geophys. J. R. Astron. Soc. **58**, 261, 1978

Červený, V., Popov, M.M., Psencik, I.: Computation of seismic wave fields in inhomogeneous media, Gaussian beam approach. Geophys. J. R. Astron. Soc. **70**, 109–128, 1982

Chapman, C.H.: A first-motion alternative to geometrical ray theory. Geophys. Res. Letts. **3**, 153–156, 1976

Chapman, C.H.: A new method for computing synthetic seismograms. Geophys. J.R. Astron. Soc. **54**, 481–518, 1978

Chapman, C.H., Drummond, R.: Body-wave seismograms in inhomogeneous media using Maslov Asymptotic Theory. Bull. Seismol. Soc. Am. **72**, 277–318, 1982

Forsyth, D.W.: The early structural evolution and anisotropy of the oceanic upper-mantle. Geophys. J. R. Astron Soc. **43**, 103–162, 1975

Frazer, L.N., Phinney, R.A.: The theory of finite frequency synthetic seismograms in inhomogeneous elastic media. Geophys. J. R. Astron. Soc. **63**, 691–717, 1980

Gilbert, F., Knopoff L: The directivity problem for a buried line source. Geophysics **26**, 626–634, 1961

Given, J.: Inversion of body-wave seismograms for upper mantle structure. Ph.D. Thesis, California Institute of Technology, Pasadena, California 1984

Grand, S.P., Helmberger, D.V.: Upper mantle shear structure beneath the northwest Altantic Ocean. J. Geophys. Res. **89**, 11465–11475, 1984a

Grand, S.P., Helmberger, D.V.: Upper mantle shear structure of North America. Geophys. J.R. Astron. Soc. **76**, 399–438, 1984b

Helmberger, D.V.: Numerical seismograms of long-period body waves from seventeen to forty degrees. Bull. Seismol. Soc. Am. **63**, 633–646, 1973

Helmberger, D.V.: Theory and Application of Synthetic Seismograms. Proceedings of the International School of Physics, Course LXXXV, H. Kanamori and E. Boschi, eds. North Holland Press 1983

Helmberger, D., Malone, S.: Modeling local earthquakes as shear dislocations in a layered half space. J. Geophys. Res. **80**, 4881–4888, 1975

Hong, T.L., Helmberger D.V.: Generalized ray theory for dipping structure, Bull. Seismol. Soc. Am. **67**, 995–1008, 1977

Hong, T.L., Helmberger D.V.: Glorified optics and wave propagation in non-planar structure. Bull. Seismol. Soc. Am. **68**, 1313–1330, 1978

Hudson, J.A.: *SH* waves in a wedged-shaped medium. Geophys. J. R. Astron. Soc. **7**, 517–546, 1983

Madariaga, R., Papadimitriou, P.: Gaussian beam modeling of upper mantle phases, submitted to Annales Geophysicae, 1984

Müller, G: Approximate treatment of elastic body waves in media with spherical symmetry. Geophys. J. R. Astron. Soc. **23**, 435–449, 1971

Vidale, J., Helmberger D.V., Clayton, R.W.: Finite-difference seismogram for *SH*-waves. Bull. Seismol. Soc. Am. 1984, (in press)

Wesson, R.L.: A time integration method for computation of the intensities of seismic rays. Bull. Seismol. Soc. Am. **60**, 307–316, 1970

Wiggins, R.A.: Body wave amplitude calculations, II. Geophys. J. R. Astron. Soc. **46**, 1–10, 1976

Received February 20, 1985; revised version June 17, 1985
Accepted June 21, 1985